

PCCP

Accepted Manuscript



This is an *Accepted Manuscript*, which has been through the Royal Society of Chemistry peer review process and has been accepted for publication.

Accepted Manuscripts are published online shortly after acceptance, before technical editing, formatting and proof reading. Using this free service, authors can make their results available to the community, in citable form, before we publish the edited article. We will replace this *Accepted Manuscript* with the edited and formatted *Advance Article* as soon as it is available.

You can find more information about *Accepted Manuscripts* in the [Information for Authors](#).

Please note that technical editing may introduce minor changes to the text and/or graphics, which may alter content. The journal's standard [Terms & Conditions](#) and the [Ethical guidelines](#) still apply. In no event shall the Royal Society of Chemistry be held responsible for any errors or omissions in this *Accepted Manuscript* or any consequences arising from the use of any information it contains.

Spatially Organized Partial Synchronization Through the Chimera Mechanism in a Network of Electrochemical Reactions

Mahesh Wickramasinghe and István Z. Kiss

Department of Chemistry, Saint Louis University, 3501 Laclede Avenue,
St Louis, MO 63103, USA.

Detailed experimental and numerical results are presented about the pattern formation mechanism of spatially organized partially synchronized states in a networked chemical system with oscillatory metal dissolution. Numerical simulations of the reaction system are used to identify experimental conditions (heterogeneity, network topology, and coupling time-scale) under which the chemical reactions, that take place on a network, split into coexisting coherent and incoherent domains through the chimera mechanism. Experiments are carried out with a network of twenty electrodes arranged in a ring with seven nearest neighbor couplings in both directions along the ring. The patterns are characterized by analyzing the oscillation frequencies and entrainments to the mean field of the phases of oscillations. The chimera state forms from two domains of elements: the chimera core in which the elements have identical frequencies and are entrained to their corresponding mean field, and the chimera shell where the elements exhibit desynchrony with each other and mean field. The experiments point out the importance of low level of heterogeneities (e.g., surface conditions) and optimal level of coupling strength and time-scale as necessary components for the realization of the chimera state. For systems with

large heterogeneities, a ‘remnant’ chimera state is identified where the pattern is strongly affected by the presence of frequency clusters. The exploration of dynamical features with networked reactions could open ways for identification of novel types of patterns that cannot be observed with reaction diffusion systems (with localized interactions) or with reactions under global constraints, coupling, or feedback.

1. Introduction

Activity patterns originating from competing chemical reactions in spatially extended systems are ubiquitous in nature and underlie important physiological processes, e.g., in circadian rhythms, neuron electrophysiology, or calcium signaling.¹⁻⁴ The general features of patterns often can be explored with relatively simple chemical reactions^{2,3}; these studies facilitate the development of experimental and theoretical tools for effective characterization of complex, multiscale systems. One important class of patterns can arise in discrete reaction units with oscillatory chemical reactions. The units can interact with each other through mass transfer, electrical coupling, or some external constraint. Examples include coupled continuous, fed stirred tank reactor systems (CSTR) of Belousov – Zhabotinsky (BZ) oscillators,⁵⁻⁸ pH oscillators,⁹ or biochemical oscillators¹⁰; large population of units can be obtained from BZ - beads,^{11,12} BZ - microwell arrays,¹³ or in BZ - micro¹⁴ and - nanoscale¹⁵ systems. In heterogeneous systems, electrochemical reactions on multielectrode arrays can be used for investigations of oscillatory patterns.¹⁶⁻²¹ A common spatiotemporal pattern observed with weakly, globally coupled oscillatory units is cluster formation²²; the population splits up into groups in which the kinetic trajectories are identical but differ

from those of the other groups. A one-cluster state obtained from slightly heterogeneous oscillators (which have a frequency distribution) can develop through Kuramoto^{19,23} or quorum¹² transition. Two and higher order cluster states have been observed with electrochemical,²⁴⁻²⁶ BZ,^{27,28} and heterogeneous catalytic²⁹ reaction systems.

Another type of self-organized pattern consisting of co-existing phase coherent and phase incoherent elements, known as the chimera state, was found to exist in numerical simulations and theoretical studies of networked units.^{17,27,30-37} While with local and global interactions the typical behaviors are various types of reaction waves and clusters, respectively, with network coupling novel patterns are expected to arise because of the large variety of possible modes of spatiotemporal variations. Experiments in chemical BZ bead reaction,^{27,35} electrochemical corrosion¹⁷ and silicon dissolution reaction^{38,39}, mechanical pendulum system,³⁶ and feedback modulated liquid crystal³⁷ and optical⁴⁰ systems have provided confirmation for the existence of the chimera patterns. The dynamical varieties of these patterns imply that there are possibly many mechanisms that can generate chimera-like structures. A striking feature of the chimera state obtained from the original Kuramoto-mechanism³⁴, is that both two locally coupled and a population of globally coupled identical oscillators form completely synchronized (one-cluster) state, while a spatially organized partially synchronized state develops in networks with symmetrical coupling topology. In a previous study,¹⁷ we provided an experimental evidence for the existence of the Kuramoto-chimera state in a non-locally coupled regular (NLR) electrochemical network of anodic nickel dissolution in sulfuric acid.

In this paper, we present a detailed study of properties of the chimera patterns in the electrochemical network system. Numerical simulations with experiment-based phase model are presented, which are used as guidance for the optimization of the experimental conditions (delay in phase interaction function, network size, connectivity) for the chimera state. The experimental system has unavoidable heterogeneity (likely due to varying surface conditions) in the form of a frequency distribution of the oscillating units; to investigate the balancing effect of coupling strength for suppression of heterogeneities due to synchronization, and enhancement of heterogeneities due to the chimera effect, we characterized the features of the chimera pattern under weak, intermediate, and strong coupling strengths. The chimera pattern occurs only transiently in the experiments; the transient and long-term behaviors of the patterns are also presented. The chimera patterns are compared to a weakly heterogeneous system with classical features, and to a more heterogeneous ‘remnant chimera’ consisting of frequency clusters. Finally, the features of the chimera patterns in the electrochemical system are compared to those of the other experimentally reported patterns in chemical and physical systems.

2. Experimental and Numerical Methods

2.1. Experimental setup

A standard three-electrochemical cell consisting of a nickel working electrode array, a Hg/Hg₂SO₄/saturated K₂SO₄ reference electrode, a platinum counter electrode, and 3 mol/L H₂SO₄ electrolyte solution were used in the experiments (figure 1a). The reactor temperature was maintained at 10 °C by a circulating bath. The electrode array was made with 1 mm spacing embedded in epoxy so that reactions take place at the end.

The electrode array was machine polished on series of sand papers (P180 - 4000). Each wire of the electrode array was connected to a potentiostat through an external resistance R_{ind} . The electrodes are polarized at a constant circuit potential V , which was set 20 mV anodic to a Hopf bifurcation to obtain stable smooth electrochemical oscillation shown in figure 1b. Currents across the external resistances were acquired at 200 Hz data acquisition rate using a National Instruments PCI 6255 data acquisition board. A typical dataset consists of 200 oscillations with 600 data points per cycle.

Non-locally coupled regular (NLR) electrochemical reaction network: A node of a network is an oscillatory nickel dissolution reaction occurring on the surface of an electrode of the array. A network edge (link) is created with a coupling resistance (R). A capacitor parallel to each coupling resistor is added to induce some delay in coupling current.⁴¹ The schematic of NLR with twenty electrodes and 140 links is shown in figure 1c. An electrode is connected to seven of its nearest neighbors (in both directions along the chain) distributing connections symmetrically. The network consists of 140 total connections to the network for twenty electrodes. The coupling strength between two oscillators is defined as inverse of coupling resistance, i.e. $K = 1/R$.

2.2. Frequency of oscillations

We use the Hilbert transform of the time series of current

$$H(t) = \frac{1}{\pi} \text{PV} \int_{-\infty}^{\infty} \frac{I(\tau) - \langle I \rangle}{t - \tau} d\tau \quad (1)$$

in defining phase⁴²

$$\phi(t) = \arctan \frac{H(t)}{I(t) - \langle I(t) \rangle} \quad (2)$$

PV in equation (1) implies that the integral should be evaluated in the sense of Cauchy principle value. $\langle \rangle$ denotes the temporal average. The frequency ω of an oscillator is obtained from a linear fit of $\phi(t)$ vs. t .

$$\omega = \frac{1}{2\pi} \left\langle \frac{d\phi}{dt} \right\rangle \quad (3)$$

2.3. Mean field phase

The mean field phase of element k in the NLR network is defined as ³⁴

$$\Theta(t) = \arctan \frac{1}{2L+1} \sum_{k-L}^{k+L} \exp(i\phi_k(t)) \quad (4)$$

where i is the complex unit, $L = 7$ is the radius of the coupling (the element indices are circular). The phase of an oscillator relative to the mean phase (phase difference) is

$$\theta(t) = \phi(t) - \Theta(t) .$$

2.4. Kuramoto Order Parameter

The amplitude of global mean field of coupled oscillators is characterized by the Kuramoto order parameter ²³ as

$$Z(t) = \left| N^{-1} \sum_{j=1}^N e^{i\phi_j(t)} \right| \quad (5)$$

where N is number of nodes of the network.

3. Results and Discussion

3.1. Numerical Simulations

The chimera pattern is first explored with simulations using phase models. The goal of the simulations is twofold. First, they reveal the dynamical characteristic of the chimera patterns later to be identified in the experiments. Second, there is a limitation in the experiments on the number of network nodes, number of links, and delay on the phase interaction function that can be achieved; the simulations are used to identify experimentally attainable conditions under which the chimera state can occur.

3. 1. 1 Model simulations with ideal phase models

Numerical simulations are performed with a ring array of N non-locally coupled phase oscillators with phases ϕ_j ($j = 1, 2 \dots N$) evolving according to the model description:⁴³

$$\frac{d\phi_j}{dt} = 2\pi\Omega_j + g \sum_{k=1}^N M_{k,j} \Gamma(\phi_k, \phi_j) \quad (6)$$

where Ω_j is natural frequency of oscillators, M is the connection matrix with elements 1 for a connection between oscillators k and j , and 0 for absence of a connection, and g is the coupling strength. Motivated by observations of Wolfrum and Omel'chenko,³¹ we started simulations on network with a population of forty identical oscillators ($N = 40$) with phase interaction function Γ given by $a \sin(\phi_k - \phi_j) + b(1 - \cos(\phi_k - \phi_j))$. Such interaction function can be observed with oscillatory behavior close to a Hopf bifurcation²³. The units are arranged on a ring; each oscillator is connected to 14 nearest neighbors oscillators (coupling range $L = 14$) on each side giving a total number of 560 links.

We present simulation results of ($N = 40, L = 14$) with setting $a = 0.01101$ and $b = -10 \times a$. The solution of equation (6) for identical

oscillators with $\Omega_j = 0.4$ Hz and $g = 0.26$ exhibits features of the typical chimera behavior. Phase dynamics of 211 cycles after the initial transient behavior were analyzed for the chimera behavior. As illustrated in figure 2a, the frequencies of oscillator-network are organized in coherent phase-locked and desynchronized domains. Nine oscillators display phase synchronization with frequencies 0.374 Hz. The spatial organization of the desynchronized oscillators leads to the semi-circle frequency variation as a function of position along the ring; such variation is characteristic of the chimera state³⁴.

Phases of oscillators relative to the mean field [$\theta(t)$] are illustrated in figure 2c. Phases are bounded for nine oscillators (1- 4, 36 - 40 in figure 2c) forming the synchronized ‘core’ and phases of the rest exhibit phase slipping behavior leading to the domain of the desynchronized ‘shell’. Shell oscillators (e.g. 5 and 35) neighboring the synchronized core display few phase slips. Phase slipping gradually increases from edges to the middle of the shell (20th oscillator); hence, shell-oscillators away from the core exhibit little synchrony with the neighboring elements. Without coupling each oscillator exhibits a natural frequency of 0.4 Hz. The coupling desynchronizes the shell oscillators; the most desynchronized oscillator exhibits a decreased frequency of 0.318 Hz.

The chimera state is obtained from a desynchronized initial condition when the Kuramoto order parameter increases from the initial value of $Z = 0.14$ (no synchronization) to $Z = 0.76$ (partial synchronization) as shown in figure 2b. After a transient time (about 10,000 oscillations), the chimera state breaks up and converges to a fully synchronized state where the order parameter is 1 (see figure 2b). This observation confirms the previous findings³¹, that in the given configuration the chimera state is a

long transient state. Extensive simulations with several networks sizes showed that the transient time exponentially increases with network size.³¹

The simulations thus reveal that with a phase model that contains small positive, phase attracting) sinusoidal and large cosine harmonics in the interaction function, the chimera state can be realized. As quantitative means for the pattern characterization, we can analyze the variation of frequency and a position dependent synchronization to the mean field along the chain. The chimera state exhibits as a form of transient, spatially organized partially synchronized state with a group of core elements that are synchronized, and a group of shell elements that are desynchronized.

3.1.2. Model simulations with experiment-based phase models

The direct realization of the chimera state through the Kuramoto mechanism presented in section 3.1.1 has many experimental obstacles including

(i) The oscillators are heterogeneous, i.e., there is a distribution of the natural frequencies. Even relatively small extent of heterogeneity is capable of destroying the pattern⁴⁴.

(ii) The phase interaction function in equation (6), which was experimentally measured previously^{24,41}, has weak higher harmonics. The impact of these small higher harmonics on the formation of the chimera state needs to be explored.

(iii) The experimental conditions must be realized in such a manner that there is a large ratio of cosine and sine functions.³³ The ratio in a given system depends on the property of the oscillator (e.g., timing of inherent kinetic feedback loops, values of rate constants, and other parameters such as resistance and potential for an electrochemical

system) and the type of coupling (difference or differential coupling, or through coupling delay).

(iv) The relatively large number of network links (>500) are not possible to realize in our experiments. The number of links and the number of electrodes should be kept below 200 and 80, respectively.

In the first step, our objective was to reduce the total number of links to a value that we can realize in the design of the experiments while the solution to equation (6) exhibits features of the chimera state. A series of simulations was carried out for different network sizes and number of connections ($N = 30, L = 11$), ($N = 30, L = 11$), ($N = 30, L = 14$), ($N = 20, L = 5$), ($N = 20, L = 7$), ($N = 18, L = 7$), and ($N = 16, L = 5$) with homogeneous oscillators (with $\Omega = 0.4$ Hz). These simulations indicated that the chimera state can robustly exist with a network size of 20 oscillators with 7 nearest neighbor coupling ($N = 20, L = 7$). The network is constructed from 140 total connections, which is below the experimental limit. The simulations show that a chimera state similar to that observed in section 3.1.1, but with a shorter lifetime of about 200 oscillations.

In the next step, we considered a heterogeneous oscillator system where the natural frequencies of oscillators (Ω_j) were chosen from a set of experimental frequencies of current oscillations in Ni electrodisolution reaction (with mean frequency of 0.3969 Hz, standard deviation of 0.1 mHz, and range of 0.5 mHz). As it was described previously¹⁹, simple difference coupling between the electrodes (implemented through cross resistors, R) results in a phase model with pure sinusoidal component. However, a differential coupling (obtained with cross-capacitors, C) gives phase interaction function

with predominant cosine components. After several experimental trials for RC combinations, we measured a phase interaction function

$$\begin{aligned} \Gamma(\phi_k, \phi_j) = & 0.00026\pi \sin(\phi_k - \phi_j) - 0.0027\pi [1 - \cos(\phi_k - \phi_j)] \\ & + 0.0003\pi \sin(2(\phi_k - \phi_j)) - 0.0002\pi [1 - \cos(2(\phi_k - \phi_j))] \end{aligned}$$

under the coupling configuration $R = 50 \text{ k}\Omega$ and $C = 48 \text{ }\mu\text{F}$ in a system of two coupled oscillators with a 15 mHz natural frequency difference. (The experimental determination of interaction function in the Ni/H₂SO₄ electrochemical system is described elsewhere.⁴¹) This interaction function has a $|\cos(\Delta\phi)|/|\sin(\Delta\phi)|$ coefficient ratio of 10; very close to the $|a|/|b|$ ratio in the ideal phase model with $N = 40$, $L = 14$ in section 3.1.1.

Simulation results of the ($N = 20$, $L = 7$) NLR network are shown in figure 3 for heterogeneous oscillators having natural frequency distribution range of 0.5 mHz (figure 3a, open circle) and coupling strength of $g = 0.503$. Simulated dynamics were analyzed for chimera behavior in the time frame $t = 300 - 820$ (204 cycles) when Kuramoto order parameter was around $Z(t) = 0.78$ (figure 3b). Eight oscillators, 1 - 4 and 17 - 20, form the synchronized core with a frequency of 0.395 Hz and the rest, oscillators 5 - 16, are in the desynchronized shell. The average frequency deviation of the shell is about 5 mHz from the core oscillators; 10 times the range of natural frequency distribution. Note that even though shell oscillators such as 7 - 10 appear to have similar frequencies in figure 3a, they are not synchronized to their mean field (figure 3c). The same explanation can be drawn for oscillators 5 - 6 and 11 - 13 in figure 3a. Core-oscillators are phase locked and shell-oscillators exhibit phase slipping behavior with respect to the mean field phase during the chimera state. Oscillators become fully phase synchronized when the order parameter reaches $Z = 1$ as shown in figure 3b after about 300 oscillation.

Simulations were also carried out with the same 20-oscillator NLR network for weak coupling strength at $g = 0.005$ (not shown). The chimera behavior was absent.

The simulations thus reveal that chimera state is attainable with a 20-oscillator ring network with each element coupled to 7 nearest neighbors to the left and right along the chain. The experiment-based phase models show that the chimera state is robust against heterogeneities of about 0.5 mHz. However, a sufficiently large coupling strength needs to be applied to suppress the heterogeneities. The expected lifetime of the experimental chimera state is on the order of 100 oscillations.

3.2. Experiments

All experiments were performed with a non-local regular network of 20 reaction units (electrodes or nodes) with 140 connections. The difference between the experiments was the applied coupling strength and the extent of the heterogeneities (experimentally observed as the range of natural frequency distribution) of the electrodes.

3.2.1. Chimera state of non-locally coupled smooth oscillators

Without any added coupling, the current oscillation of each electrode has a slightly different frequency resulting in a distribution with a range of about 16 mHz (see figure 4a). The frequency distribution is likely caused by surface heterogeneity: The natural frequencies of each wires are reproducible between subsequent repolishing within about 1-2 mHz error; this error is smaller than the observed range, which indicates the importance of metal impurities in the course of the dissolution process. In addition, the oscillation frequency also changes slowly with time (about few mHz/hour) and thus

additional properties (spatial oxide film heterogeneities and oxide layer thickness) could also contribute to the frequency distribution. Surface heterogeneities also played role in the dynamics of H_2O_2 reduction on p-CuInSe₂ electrode; the inhomogeneously growing passivating surface layer formed islands, and the islands grew with time resulting in a time-transient dynamical response.⁴⁵ Heterogeneities thus could occur for many electrochemical oscillatory systems and their extent and time variation could significantly impact the observed dynamics.

Experiments were performed by small adjustments to individual resistors R_{ind} , which narrowed the natural frequency range of oscillators from 16 mHz to 0.5 mHz (see figures 4a - b and 5b), before tuning on coupling. This ensured that the chimera mechanism was responsible for the intensified incoherence among ‘shell’ oscillators. As the numerical simulations indicated, we employ combination of capacitor and resistor in parallel as a coupling element so that the coupling current across the resistor is delayed by the capacitance.

When coupling was turned on, a group of synchronized ‘chimera-core’ electrodes, elements 1- 4 and 17- 20 in figure 5a, and a group of desynchronized ‘shell’ electrodes, elements 5-16 in figure 5a, were observed for 84 cycles. (This chimera state is the same as published previously¹⁷; here we review the results for subsequent comparisons at various coupling strengths and heterogeneities.) The eight core electrodes have very similar currents (see figure 5a) and deviations arise outside the core region. Eight core oscillators are synchronized to a frequency of 0.389 Hz and all shell elements have lower frequencies than the core frequency. The frequency distribution in figure 5b reveals that shell elements are desynchronized and they form a lower semi-circle as a

function of position confirming the numerical simulation results. The strong incoherence between the core and the shell domains broadens the initial 0.5 mHz frequency range to about 18 mHz. This frequency enlargement indicates the presence of the chimera symmetry breaking mechanism.³³ A plot of phase of each oscillator relative to the mean field phase $[\Theta(t)]$ in figure 5d further confirms the chimera behavior of the system. Phases of core oscillators are locked to the mean field phase (therefore, phase difference is zero) while phases of the shell oscillators exhibit phase slipping behavior (time sequences of phase locking is interrupted with a relatively quick 2π phase slip). Note that although many shell elements have similar frequencies, they are not synchronized to the mean field. Shell oscillators near the core display only 1- 2 phase slips in 84 cycles as shown in figure 5c while shell elements away from the core exhibit about 4 phase slips. Figure 5c shows Kuramoto order parameter as a function time; the system exhibits partial synchrony with a mean value of $Z = 0.73$. After the break-up of the chimera state the system typically approaches full synchrony with $Z = 1$ (not shown). Therefore, the chimera state in the experiment is a long transient state. The transient nature of the experimental system could arise due to drifting natural frequencies of oscillators as well; however, as it was shown numerically with the phase equation (6) in section 3.1, the chimera state in the given coupling configuration was an inherent transient behavior for a finite number of oscillators.

The chimera state was stable for about 80 - 100 cycles and was observed in 9 out of 14 experiments. Most successful attempts (6/9) were made during the first four hours when natural frequency-drifts of oscillators were minimal. In remaining five experiments,

most (4/5) done after four hours, less than 5 oscillators exhibited synchronization in 100 cycles.

The experiments thus confirm that the chemical reaction system, within experimental limitations, exhibits a very robust partially synchronized state with behavioral characteristics identical to the predicted chimera state. The coupling induces co-existing synchronized and desynchronized states even in a symmetrical network. Although the lifetime of the chimera state is relatively short (about 100 oscillations), it is comparable to that obtained from numerical simulations. The most unexpected feature of the partially synchronized state is that the coupling induces synchronization among core elements; nonetheless, the very same coupling enhances frequency differences for shell elements. Because the coupling among the oscillators was induced with current through a parallel resistance/capacitance element, the coupling signal has a timescale of $RC = 2.35$ s. This coupling time-scale matches the time scale (period) of the oscillatory process (2.5s). Similar time-scale matching has been observed with chimera state observed with the coupled pendulum system³⁶. The electrochemical experiments thus confirm the idea proposed in the pendulum chimera system³⁶ about the prevalence of the mechanical analogy of development of chimera state as a competition between different synchronization modes in a coupling parameter region centered around the resonance curve where the uniform synchronization breaks up.

3. 2. 2 Chimera state at weak coupling strength

A weak form of chimera behavior was observed with a 17% ($R = 600$ k Ω , $C = 4.7$ μ F) decrease in the coupling strength in comparison to the chimera state presented in the

previous section. (To minimize practical difficulties the capacitance C was kept constant in the experiments). The chimera behavior is obtained for 100 cycles having six electrochemical oscillators (1, 2, 17- 20) in the synchronized core with frequency of 0.403 Hz; the rest oscillators are in the desynchronized shell with frequency distribution range of 14 mHz as illustrated in figure 6a. Weakening the coupling strength thus diminishes the size of the core of the chimera state. A well-defined semi-circle frequency distribution is not observed for weak coupling. This chimera state was obtained when the Kuramoto order parameter maintained an average value of $Z = 0.85$ as shown in figure 6b. In the experiment with stronger coupling in section 3.2.1, we observed that the number of phase slips increases gradually from both edges of the core to the middle of the shell. However, under weak coupling, we can see that from the edge electrode 17 (no phase slip) of the chimera core, there are 1- 2 phase slips for chimera shell elements 16 - 12, three phase slips for element 11 - 10, and four phase slips for element 8; the trend is disrupted by element 9 which exhibits only one phase slip (see figure 6c). Starting from the other core edge, electrodes 3 - 7 all exhibit 2 - 3 phase slips. We thus see that the number of phase slips from the chimera core to the center of the shell elements increases in a statistical manner and exhibits strong asymmetry; these results indicate that the pattern is affected by the heterogeneity of the oscillators that are not fully suppressed at the weak coupling. The spatially ordered partially synchronized state was difficult to obtain with weak coupling; the presented example is the only experiment that produced chimera state in seven trials. In other experiments, electrochemical oscillators were weakly synchronized without apparent spatial organization during a period of 100 cycles.

3. 2. 3 Chimera state at strong coupling strength

The chimera state was observed for 190 cycles with a relatively strong coupling resistance $R = 390 \text{ k}\Omega$ (capacitance $C = 4.7 \text{ }\mu\text{F}$). Figure 7a shows frequencies of oscillations. The chimera state at this strong coupling consists of a relatively large domain (1- 7, 17- 20) of the core elements. The desynchronized shell elements deviates only about 10 mHz from the synchronized core frequency of 0.381 Hz. Although the characteristic semi-circle variation of the frequencies of the shell elements is not noticeable, the system displays the prominent feature of the chimera state: the coexistence of synchronized and desynchronized groups with a clear separation of shell from the core frequencies. The center of the shell of the chimera state has the lowest frequency and the most (5) phase slips; the element at the left edge of the shell state exhibits only one phase slip. The other shell elements exhibit 2 - 3 phase slips (see figure 6c). The network exhibits chimera behavior when Kuramoto order parameter fluctuates between 1 and 0.6 (see figure 7c).

With very strong coupling (e.g., $R = 40 \text{ k}\Omega$, $C = 33\mu\text{F}$), all 20 oscillators formed one group attaining full phase synchronization.

The experiments thus show that the chimera state can be observed for a range of coupling strength. The most robust chimera pattern is observed at an intermediate coupling strength where there is a balance among three major factors that include heterogeneity suppression, core and shell element differentiation, and full synchronization. With increasing the coupling strength the domain of the core of the chimera patterns increases but remains within about 30% - 55% of the total population.

3. 2. 4 Long-term behavior of the NLR electrochemical network

The experimental chimera state, which closely resembles to the numerical simulation, lasted under intermediate coupling strength for about 100 oscillatory cycles. A long-term behavior (including the initiation and the termination) of the dynamics at intermediate coupling strength conditions $R = 499 \text{ k}\Omega$ ($C = 4.7 \text{ }\mu\text{F}$) is shown in figure 8.

The system is initiated from a desynchronized state with low value of the Kuramoto order parameter at $t = 0 \text{ s}$. When the coupling is turned on, the oscillators synchronize and quickly approach a state in which Z is close to 1 at $t = 250 \text{ s}$ (figure 8b). This fully synchronized state collapses to a chimera behavior at $t = 600$; thereby, the average Kuramoto order parameter decreases to 0.87.

Nine electrodes (4 – 7, 9 – 13) form the synchronized core with frequency 0.395 Hz as shown in figure 8a. (Element 8 exhibits only one phase slip during the time interval for the chimera state.) The chimera state was sustained for the next 215 cycles. (The conditions for the chimera state are the same as those in figure 5, however, now we analyze the chimera state for more than twice as long time interval - 215 cycles vs. 84 cycles). The maximum frequency difference between shell and core oscillators is 13 mHz. The semi-circle distribution of frequencies is not apparent compared to that of the short-term chimera behavior under the intermediate coupling strength. Inherent drifts in natural frequencies adversely affect the formation of chimera state since increasing heterogeneity in frequencies prevents the formation of chimera state. Phases of oscillators relative to the mean field phase are shown for the chimera state in figure 8c.

In the experiments the chimera state collapses after some time; this collapse often occurs through the formation of frequency clusters in which frequency of the twenty

electrodes split into several small domains (phase synchronization within a domain) as shown in figure 9. In this state, two types of frequency clusters can be observed. A chimera-core-like cluster is formed with oscillators 1-3, 6, and 17 (figure 9a-black circles); these elements are entrained to both the mean field and to each other. For example, electrode 1 is in-phase with both the mean field (figure 9c) and another chimera core element 2 (see figure 9b). (Note that because of a phase slip that occurred before the formation of the frequency clusters, the phase difference between elements 1 and 2 is 2π rad instead of zero.) In the other type of frequency cluster groups, the elements are not entrained to the mean field, but they are entrained to each other. Such clustering occurs among oscillators 12 - 15 with a common frequency 0.371 Hz. For instance, the phase difference between oscillators 13 and 14, shown in figure 9b, wiggles between 0 and 2π rad, however, the phase difference is bounded and does not grow; this leads to phase synchronization between elements 13 and 14. However, phase evolutions of both 13 and 14 are not synchronized to the mean field (figure 9c). The intermediate coupling at $R = 499 \text{ k}\Omega$ ($4.7 \text{ }\mu\text{F}$) produced three frequency clusters with frequencies 0.378 Hz (elements 4, 8, 20), 0.371 Hz (elements 12 - 15), and 0.368 Hz (elements 11, 16). Elements 5, 7, 9, 10, 18 and 19 showed no phase synchronization either to the mean field or to any other elements. Phase differences of these non-clustering oscillators exhibit phase-slipping with elements of the core cluster (figure 9b, $\Delta\phi_{1,10}$) and either pure phase slipping or mixed phase slipping and wagging with other frequency clusters.

In some long-term experiments with intermediate coupling, the chimera state is typically observed approximately for 100 cycles ($1 > Z > 0.7$) and it collapsed to a fully synchronized state ($Z = 1$) for about another 100 cycles. This alternation between chimera

and fully synchronized states appears 2 - 3 occasions during a long-term experiment, and the final state is typically a frequency clustered state.

3.2.5. Remnant chimera state with frequency clustering in heterogeneous oscillator network

Heterogeneous natural frequencies do not facilitate the formation of the chimera state strictly defined by the Kuramoto conditions.⁴⁴ The typical behavior of a heterogeneous population (with multimodal frequency distribution) with global coupling is the formation of frequency clusters⁴⁶. However, under conditions favorable for chimera states, we found that the formation of the frequency clusters is affected by chimera dynamics through a state quite similar to the terminal state shown in figure 9. Strong coupling strength at $R = 390 \text{ k}\Omega$ ($C = 4.7 \mu\text{F}$) was needed to (partially) suppress the relatively large heterogeneities (15 mHz range in natural frequency in Figure 10) of the oscillating elements. Under these conditions, five frequency clusters were obtained as illustrated in figures 10a and 10b; the clusters have frequencies $0.3966 \text{ Hz} \pm 0.1 \text{ m Hz}$ (elements 1, 2, 14 - 16), $0.3940 \text{ Hz} \pm 0.1 \text{ m Hz}$ (elements 4, 7, 9, 17 - 20), $0.3913 \text{ Hz} \pm 0.3 \text{ m Hz}$ (elements 3, 8), $0.3887 \text{ Hz} \pm 0.4 \text{ m Hz}$ (elements 11 - 13), and $0.3860 \text{ Hz} \pm 0.4 \text{ m Hz}$ (elements 5, 10). The state can be considered as a ‘remnant’ chimera state where the core of the chimera consists of elements 1- 2, 4, 7, 9, and 14 - 20. Within the core, elements 1, 2, 14 - 16 are synchronized to each other and to their mean field while the remaining elements exhibit only about two phase slips in a relatively long time of 200 oscillations (see figure 10d). Note that large domain of the chimera core consists of contiguous elements 1- 2 and 14 - 20; the other elements (4, 7, and 9) are in spatially

isolated regions away from the major domain. (We did not find evidence that the core or the shell of the chimera state was pinned to heterogeneities in an obvious manner; for example, half of the chimera core elements had similar natural frequencies, while the other half had largely different natural frequencies.) The noisy chimera shell (elements 3, 5 - 6, 8, 10 -13) is formed from 4 frequency clusters. In each cluster, the elements are synchronized to each other but not to the mean field; the typical size of the cluster varies between 1-3 elements. The elements in these frequency clusters can consist of either contiguous elements (e.g., elements 11-13) or from spatially distinct units (e.g., elements 3 and 8). The Kuramoto order parameter fluctuates strongly between 0.5 and 1 as shown in figure 10c; such fluctuating order parameters are often observed with frequency clustering⁴⁶.

4. Conclusions

In summary, we obtained spatially organized partial synchronization in a non-locally coupled electrochemical network through the Kuramoto chimera mechanism^{23, 24, 26}. An experiment-based phase modeling technique²⁴ was used to optimize the network topology (20 units on a ring, coupled to 7 nearest neighbors on both sides) and the time scale of the coupling signal (2.5 s), which matched the period of oscillations (about 2.35 s). The chimera state was most robustly observed at intermediate coupling strength where the inherent heterogeneities were suppressed by the coupling while the chimera symmetry breaking mechanism was responsible for desynchronization of the shell elements. Within the coupling range that supported formation of the chimera state, the core (synchronized) portion of the pattern increased in size with increasing the coupling

strength. Increasing heterogeneity among electrochemical oscillators did not favor developing the chimera state. However, an important fingerprint of chimera behavior was found with the heterogeneous elements: in one of the frequency cluster, which is typically composed of contiguous elements, the units are not only synchronized among each other, but also to their corresponding mean field. This finding could facilitate the identification of ‘remnant’ or ‘noisy’ chimera states (e.g., in biological system) where the inherent heterogeneities are relatively strong. We note, however, that the calculation of a quantity for the extent of synchronization to the mean field requires the complete identification of the network topology, which can be a tedious task in systems where the links are difficult to visualize, e.g., with cellular systems.⁴⁷

The chimera pattern obtained with the electrochemical experiment can be compared to those obtained with the BZ bead^{35, 48} and the silicon dissolution system^{38, 39}. The chimera state with the BZ bead system was observed with a spatially distributed illumination feedback that implemented a NLR or a two-group network of elements.^{35, 48} A major conclusion of the BZ bead experiments is that the chimera state has features that differ significantly from those obtained with phase-oscillator models. Most notably, the presence of clustering (which was reported with global feedback) could play an important role in the desynchronization mechanism of the shell elements. The chimera-like state with the silicon dissolution experiments^{38, 39} arises as competition between various cluster state and sizes, and thus can be observed with pure global coupling. In addition, the system should have sufficiently large nonlinearity (most likely through the coupling mechanism) to support the co-existence of domains of the vastly different types of cluster states.³⁸ In our experiments the mechanism for chimera state could be attributed to the

original Kuramoto mechanism³⁴; the mechanism can be clearly identified because of the existence of experiment-based, predictive phase models for electrochemical oscillators.^{24, 49} The experiments presented with the Ni electrodisolution system here are examples of pattern formation uniquely induced by the presence of network, and not a representation of a dynamical behavior (e.g., clustering) in the presence of network. Categorization of the different types of chimera-like behaviors is an important future direction for physical, chemical, and biological oscillatory systems.

Acknowledgements

This material is based upon work supported by the National Science Foundation under Grant No. CHE-0955555. Acknowledgement is made to President's Research Fund of Saint Louis University for support of this research.

References

- 1 A. T. Winfree, *The geometry of biological time*, Springer-Verlag, New York, 1980.
- 2 I. R. Epstein and J. A. Pojman, *An Introduction to Nonlinear Chemical Dynamics: Oscillations, Waves, Patterns, and Chaos*, Oxford University Press, USA, 1998.
- 3 K. Showalter and R. Kapral, *Chemical Waves and Patterns (Understanding Chemical Reactivity)*, Kluwer, Dordrecht, 1995.
- 4 I. Z. Kiss and J. Hudson, *AIChE J.*, 2003, **49**, 2234-2241.
- 5 M. Marek and I. Stuchl, *Biophys. Chem.*, 1975, **3**, 241-248.
- 6 M. F. Crowley and I. R. Epstein, *J. Phys. Chem.*, 1989, **93**, 2496-2502.

- 7 J. Weiner, R. Holz, F. W. Schneider and K. Bar-Eli, *J. Phys. Chem.*, 1992, **96**, 8915-8919.
- 8 M. J. B. Hauser and F. W. Schneider, *J. Chem. Phys.*, 1994, **100**, 1058-1065.
- 9 O. Pesek, L. Schreiberova and I. Schreiber, *Phys. Chem. Chem. Phys.*, 2011, **13**, 9849-9856.
- 10 A. Lekebusch and F. W. Schneider, *J. Phys. Chem. B*, 1997, **101**, 9838-9843.
- 11 H. Fukuda, H. Morimura and S. Kai, *Physica D*, 2005, **205**, 80-86.
- 12 A. F. Taylor, M. R. Tinsley, F. Wang, Z. Y. Huang and K. Showalter, *Science*, 2009, **323**, 614-617.
- 13 T. Okano and K. Miyakawa, *Phys. Rev. E*, 2009, **80**, 026215.
- 14 M. Toiya, V. K. Vanag and I. R. Epstein, *Angew. Chem. Int. Ed.*, 2008, **47**, 7753-7755.
- 15 V. K. Vanag and I. R. Epstein, *Phys. Rev. Lett.*, 2001, **87**, 228301.
- 16 M. Wickramasinghe and I. Z. Kiss, in *Engineering of Chemical Complexity*, World Scientific New Jersey, 2013, pp. 215-236.
- 17 M. Wickramasinghe and I. Z. Kiss, *PLoS ONE*, 2013, **8**, e80586.
- 18 I. Z. Kiss and J. L. Hudson, *Chaos*, 2003, **13**, 999-1009.
- 19 I. Z. Kiss, Y. M. Zhai and J. L. Hudson, *Science*, 2002, **296**, 1676-1678.
- 20 A. Karantonis, M. Pagitsas, Y. Miyakita and S. Nakabayashi, *Electrochim. Acta*, 2005, **50**, 5056-5064.
- 21 A. Karantonis, Y. Miyakita and S. Nakabayashi, *Phys. Rev. E*, 2002, **65**, 046213.

- 22 S. C. Manrubia, A. S. Mikhailov and D. H. Zanette, *Emergence of Dynamical Order: Synchronization Phenomena in Complex Systems*, World Scientific, Singapore, 2004.
- 23 Y. Kuramoto, *Chemical Oscillations, Waves, and Turbulence*, Dover, Mineola, New York, 2003.
- 24 I. Z. Kiss, Y. M. Zhai and J. L. Hudson, *Phys. Rev. Lett.*, 2005, **94**, 248301.
- 25 W. Wang, I. Z. Kiss and J. L. Hudson, *Chaos*, 2000, **10**, 248-256.
- 26 H. Varela, C. Beta, A. Bonenfant and K. Krischer, *Phys. Chem. Chem. Phys.*, 2005, **7**, 2429-2439.
- 27 A. F. Taylor, M. R. Tinsley, F. Wang and K. Showalter, *Angew. Chem. Int. Edit.*, 2011, **50**, 10161-10164.
- 28 V. K. Vanag, L. Yang, M. Dolnik, A. M. Zhabotinsky and I. R. Epstein, *Nature*, 2000, **406**, 389-391.
- 29 M. Kim, M. Bertram, M. Pollmann, A. von Oertzen, A. S. Mikhailov, H. H. Rotermund and G. Ertl, *Science*, 2001, **292**, 1357-1360.
- 30 M. Wolfrum, O. E. Omel'chenko, S. Yanchuk and Y. L. Maistrenko, *Chaos*, 2011, **21**, 013112.
- 31 M. Wolfrum and O. E. Omel'chenko, *Phys. Rev. E*, 2011, **84**, 015201.
- 32 O. E. Omel'chenko, M. Wolfrum and Y. L. Maistrenko, *Phys. Rev. E*, 2010, **81**, 065201.
- 33 D. M. Abrams and S. H. Strogatz, *Phys. Rev. Lett.*, 2004, **93**, 174102.
- 34 Y. Kuramoto and D. Battogtokh, *Nonl. Phen. Compl. Syst.*, 2002, **5**, 380-385.
- 35 M. R. Tinsley, S. Nkomo and K. Showalter, *Nature Physics*, 2012, **8**, 662-665.

- 36 E. A. Martens, S. Thutupalli, A. Fourriere and O. Hallatschek, *Proc. Natl. Acad. Sci. U. S. A.*, 2013, **110**, 10563-10567.
- 37 A. M. Hagerstrom, T. E. Murphy, R. Roy, P. Hoevel, I. Omelchenko and E. Schoell, *Nat. Phys.*, 2012, **8**, 658-661.
- 38 L. Schmidt, K. Schönleber, K. Krischer and V. García-Morales, *Chaos*, 2014, **24**, 013102.
- 39 K. Schoenleber, C. Zensen, A. Heinrich and K. Krischer, *New J. Phys.*, 2014, **16**, 063024.
- 40 L. Larger, B. Penkovsky and Y. Maistrenko, *Phys. Rev. Lett.*, 2013, **111**, 054103.
- 41 M. Wickramasinghe and I. Z. Kiss, *Phys. Rev. E*, 2013, **88**, 062911.
- 42 A. S. Pikovsky, M. G. Rosenblum and J. Kurths, *Synchronization: A Universal Concept in Nonlinear Sciences*, Cambridge University Press, Cambridge, 2001.
- 43 S. H. Strogatz, *Physica D*, 2000, **143**, 1-20.
- 44 C. R. Laing, *Chaos*, 2009, **19**, 013113.
- 45 G. Neher, L. Pohlmann and H. Tributsch, *J. Phys. Chem.*, 1995, **99**, 17763-17771.
- 46 A. S. Mikhailov, D. H. Zanette, Y. M. Zhai, I. Z. Kiss and J. L. Hudson, *P. Natl. Acad. Sci. USA*, 2004, **101**, 10890-10894.
- 47 O. Sporns, *Ann. N. Y. Acad. Sci.*, 2011, **1224**, 109-125.
- 48 S. Nkomo, M. R. Tinsley and K. Showalter, *Phys. Rev. Lett.*, 2013, **110**, 244102.
- 49 I. Z. Kiss, C. G. Rusin, H. Kori and J. L. Hudson, *Science*, 2007, **316**, 1886-1889.

Figure captions:

Figure 1. Experimental setup. (a) Schematic diagram of standard three-electrode electrochemical cell with multiple working electrodes. R_{ind} : Individual resistance, R : Coupling resistance, C : Coupling capacitance. (b) Smooth current oscillations from potentiostatic anodic nickel dissolution in 3 mol/L sulfuric acid solution. (c) Non-locally coupled regular (NLR) network topology with 20 nickel electrodes and 140 links.

Figure 2. Simulation: Partial synchronization during the chimera state of forty identical phase oscillators in a non-locally coupled regular network. (a) Frequencies of oscillators without (open circles) and with (black circles) coupling. (b) Kuramoto order parameter vs. time. (c) Phase of oscillations relative to the mean field phase. $g = 0.26$, $\Omega = 0.4$ Hz, $N = 40$ in equation (6).

Figure 3. Simulation: Partial synchronization during the chimera state of twenty heterogeneous phase oscillators in a non-locally coupled regular network. (a) Open circles: Natural frequencies, black circles: frequencies of the coupled oscillators. (b) Kuramoto order parameter vs. time. (c) Phase of oscillations relative to the mean field phase. $g = 0.503$, $N = 20$ in equation (6).

Figure 4. Experiment: Frequencies of twenty smooth electrochemical oscillators without coupling among oscillators (natural frequencies). (a) Frequencies before making fine adjustment to individual resistances; this system is strongly heterogeneous with a frequency range of ± 8 mHz. (b) Frequencies after making fine adjustments to individual resistances have small range of ± 0.25 mHz.

Figure 5: Experiment: Chimera state of twenty electrochemical oscillators in the non-locally coupled network with intermediate coupling strength.¹⁷ (a) Snapshot of currents of electrodes: core oscillators (1 – 4, 17 – 20) have similar currents. (b) Frequencies of oscillators. Open circles: Natural frequencies. Black circles: Frequencies of coupled oscillators. (c) Kuramoto order parameter vs. time. (d) Phases of oscillators relative to the mean field phase. $V = 1094$ mV, $R_{\text{ind}} = 1000 \Omega$, $R = 499$ k Ω , $C = 4.7 \mu\text{F}$.

Figure 6: Experiment: Chimera state of twenty electrochemical oscillators in the non-locally coupled network with weak coupling strength. (a) Frequencies of oscillators. Open circles: Natural frequencies. Black circles: Frequencies of coupled oscillators. (b) Kuramoto order parameter vs. time. (c) Phases of oscillators relative to the mean field phase oscillators. $V = 1095$ mV, $R_{\text{ind}} = 1000 \Omega$, $R = 600$ k Ω , $C = 4.7 \mu\text{F}$.

Figure 7: Experiment: Chimera state of twenty electrochemical oscillators in the non-locally coupled regular network with strong coupling strength. (a) Frequencies of oscillators. Open circles: Natural frequencies. Black circles: Frequencies of coupled

oscillators. (b) Kuramoto order parameter vs. time. (c) Phases of oscillators relative to the mean field phase. $V = 1083$ mV, $R_{\text{ind}} = 1000 \Omega$, $R = 390$ k Ω , $C = 4.7 \mu\text{F}$.

Figure 8: Experiment: Long-term behavior of the chimera state. (a) Frequencies of oscillators. Open circles: Natural frequencies. Black circles: Frequencies of coupled oscillators. (b) Kuramoto order parameter vs. time. (c) Phases of oscillators relative to the mean field phase. $V = 1094$ mV, $R_{\text{ind}} = 1000 \Omega$, $R = 499$ k Ω , $C = 4.7 \mu\text{F}$.

Figure 9: Experiment: Terminal state of the chimera patterns in the form of a frequency clustered state. (a) Frequency of oscillators. Black circles (1-3, 6, 17): remnants of the chimera core. Diamonds (11, 16), triangles (3, 6, 20), open circles (12-15): frequency clusters. Squares (5, 7, 9, 10, 18, 19): no clustering with the core or other domains. (b) Evolution of phase difference $\Delta\phi_{m,n}(t) = \phi_m(t) - \phi_n(t)$. $\Delta\phi_{1,10}$: Phase slipping between oscillator 1 from the core and oscillator 10, $\Delta\phi_{13,14}$: phase wiggling between oscillators 13 and 14 in a frequency cluster (open circles in (a)), $\Delta\phi_{1,2}$: phase locked state between oscillator 1 and 2 in the core. (c) Phases of oscillators relative to the mean field phase. $V = 1094$ mV, $R_{\text{ind}} = 1000 \Omega$, $R = 499$ k Ω , $C = 4.7 \mu\text{F}$.

Figure 10: Experiments: Remnant chimera state with frequency clusters among heterogeneous oscillators. (a) Frequency clusters with chimera core with elements (1, 2, 14-16) and (4, 7, 9, 17-20) and shell elements (3, 8), (5, 10), (11-13) and (6). (b) Frequency of oscillators along the chain. (c) Kuramoto order parameter vs. time. (d)

Phases of oscillators relative to the mean field phase. $V = 1094$ mV, $R_{\text{ind}} = 1000 \Omega$, $R = 499$ k Ω , $C = 4.7 \mu\text{F}$.

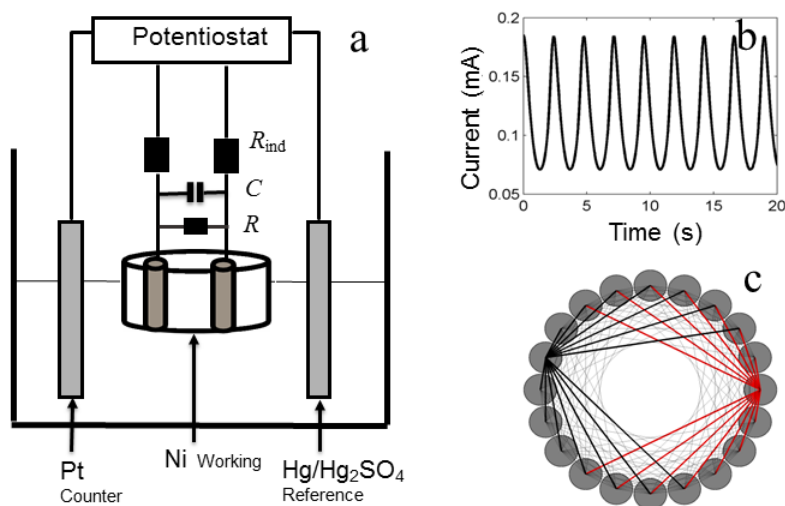


Figure 1

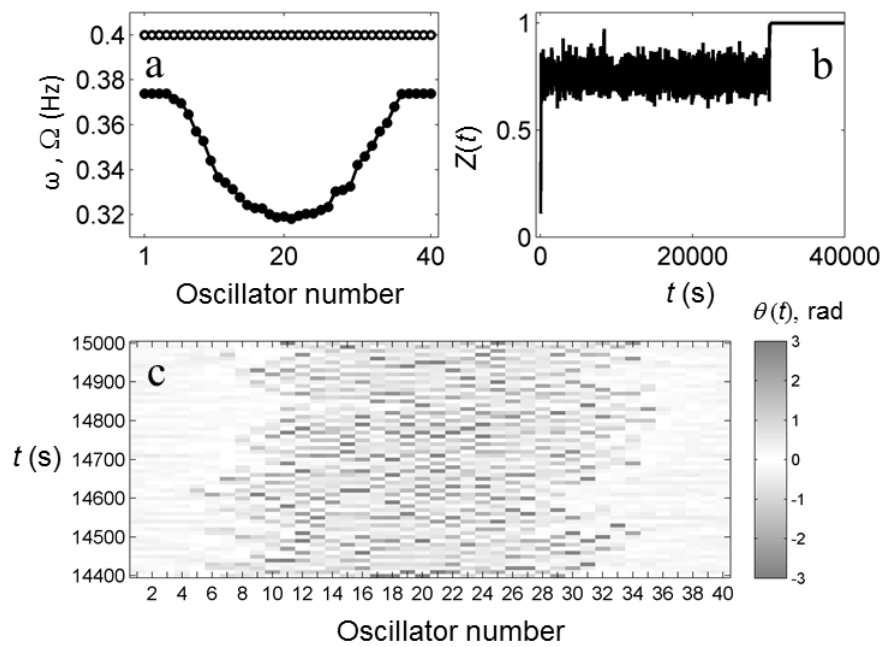


Figure 2

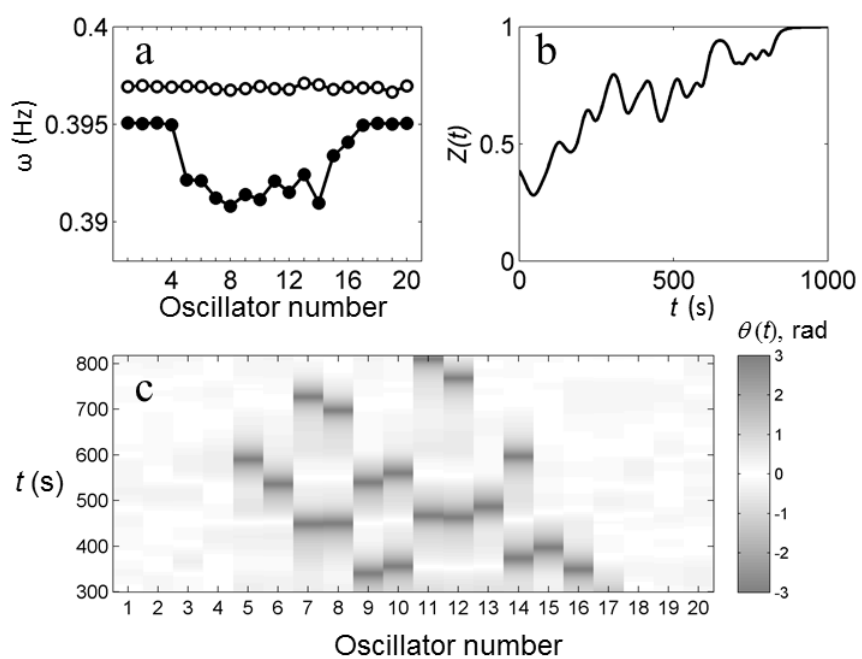
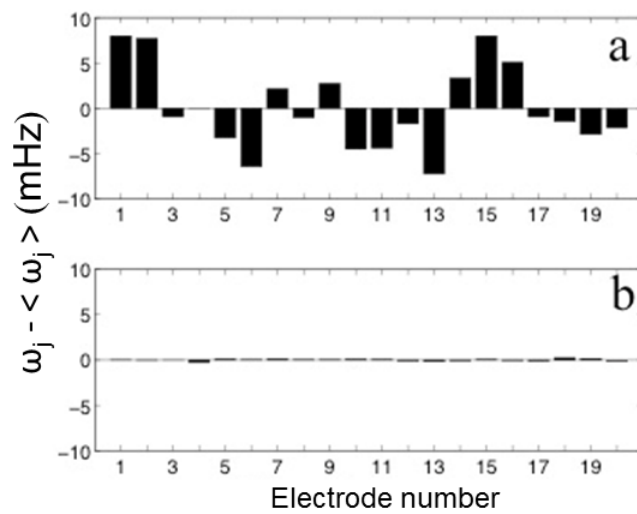


Figure 3

**Figure 4**

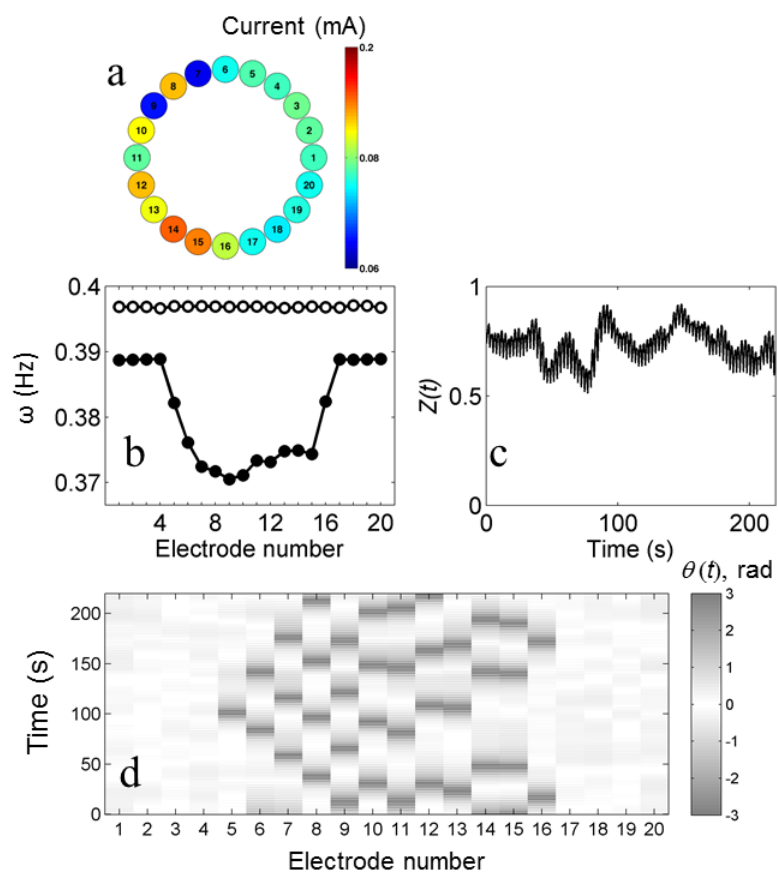
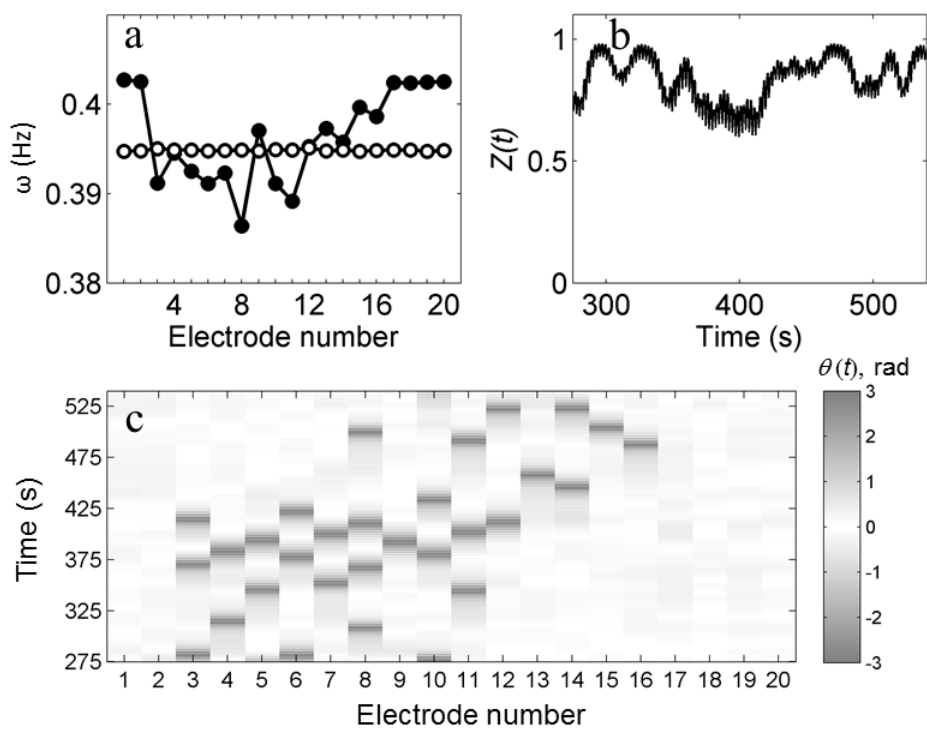


Figure 5

**Figure 6**

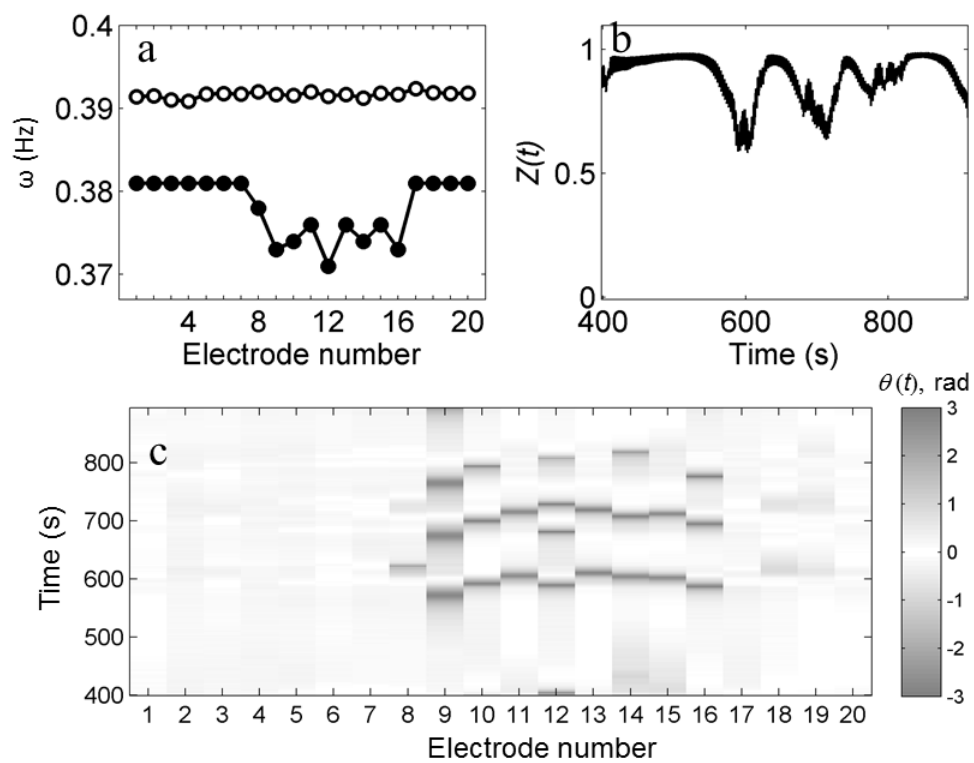


Figure 7

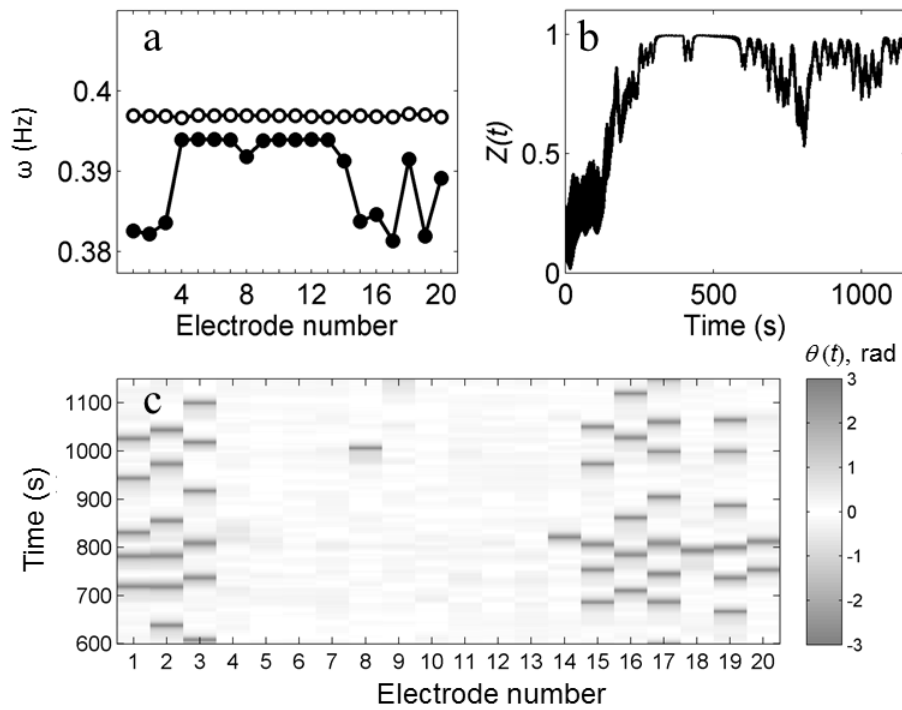


Figure 8

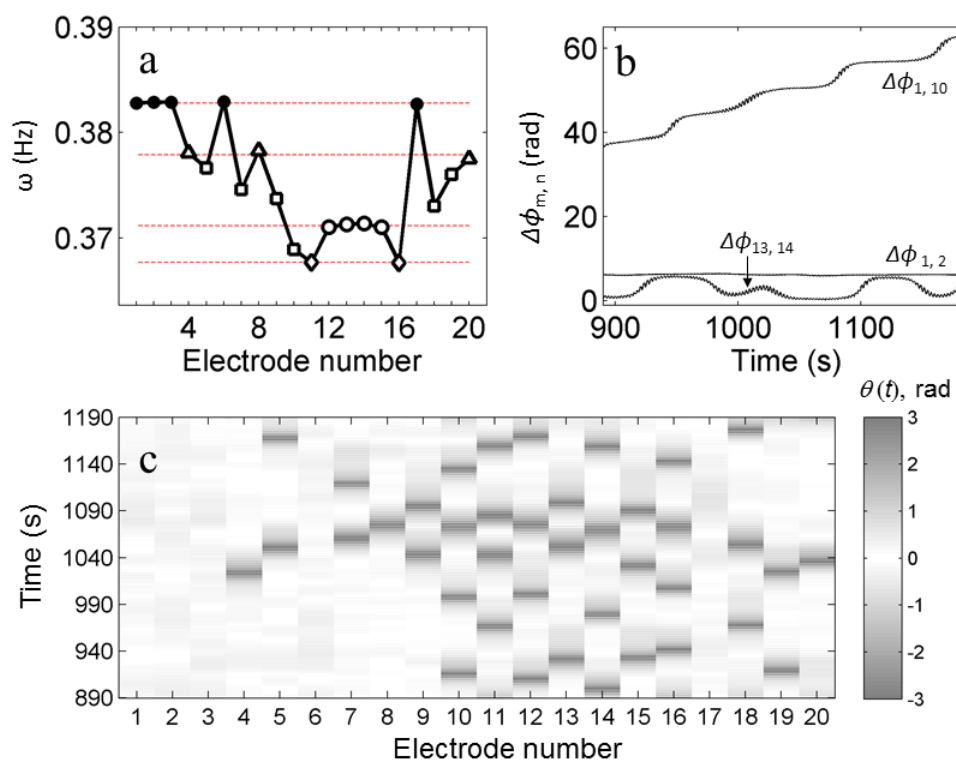


Figure 9

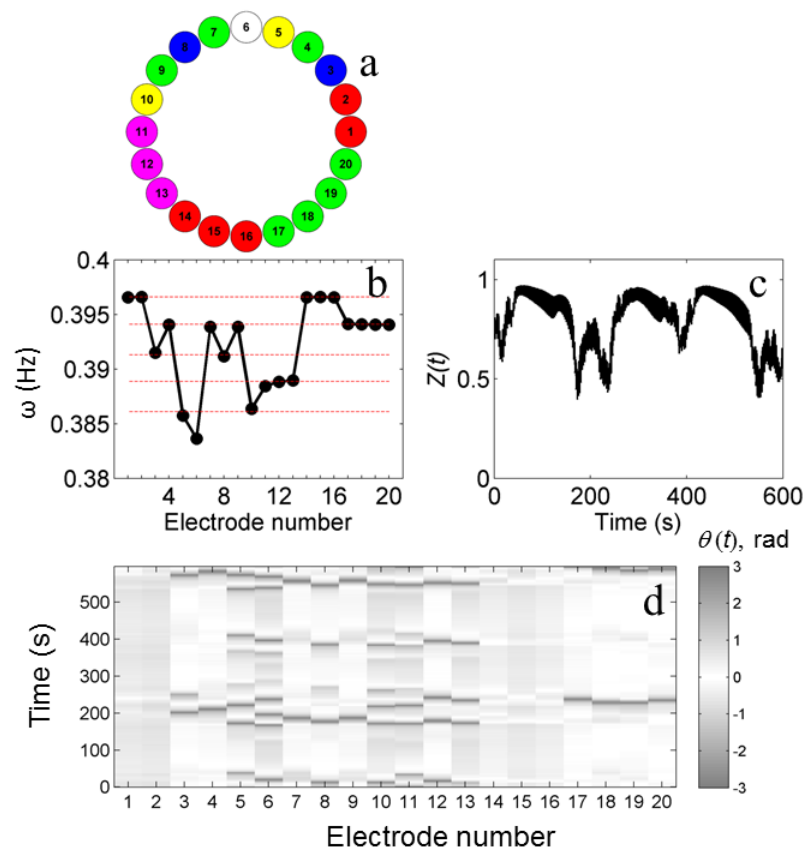
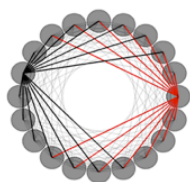
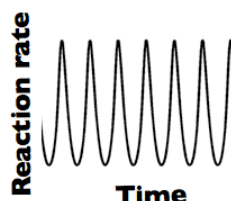
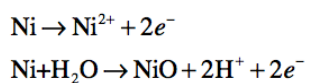


Figure 10

**Network****Chimera pattern**

TOC abstract

Oscillatory Ni dissolution reaction on a nonlocally coupled network of reaction sites produces a chimera pattern.